# RNA polymerase II activity is located on the surface of protein-rich transcription factories

**Christopher H. Eskiw*, Alexander Rapp, David R. F. Carter and Peter R. Cook‡**

Sir William Dunn School of Pathology, University of Oxford, South Parks Road, Oxford, OX1 3RE, UK

*Present address: The Babraham Institute, Babraham Research Campus, Babraham, Cambridge, CB22 3AT, UK

‡Author for correspondence (e-mail: peter.cook@path.ox.ac.uk)

*Accepted 7 April 2008*

*Journal of Cell Science 121, 1999-2007 Published by The Company of Biologists 2008*

*doi:10.1242/jcs.027250*

## Summary

**We used electron spectroscopic imaging to map nucleoplasmic transcription sites in human cells at unprecedented resolution. HeLa cells were permeabilised, nascent transcripts were extended in BrUTP by ~40 nucleotides and the resulting BrRNA immunolabelled with gold particles before structures were viewed. Nascent RNA is almost invariably associated with polymorphic and nitrogen-rich (but phosphorus-poor) structures with a diameter of ~87 nm and mass of 10 MDa (calculated by reference to nucleosomes with known numbers of phosphorus and nitrogen atoms). Structures with similar atomic signatures and diameters were observed using correlative microscopy and in unpermeabilised cells. Our results are consistent with RNA synthesis occurring on the surface of these huge protein-rich transcription factories.**

Key words: Bromo-uridine triphosphate, Electron microscopy, Electron spectroscopic imaging, Transcription

## Introduction

Transcription sites in mammalian cells can be identified in various ways. They were first localised by autoradiography after growth in [$^3$H]uridine; silver grains marking newly made [$^3$H]RNA were found over 'perichromatin fibrils' at the edge of heterochromatin (Fakan et al., 1976; Fakan, 2004). Unfortunately, pulses longer than the time taken to complete a typical transcript (~5 minutes) are required, so some grains mark transcripts that have left synthetic sites. The use of newer tags permits higher spatial and temporal resolution. For example, after allowing permeabilised cells to extend transcripts by a few nucleotides in BrUTP, the resulting BrRNA can be immunolabelled with fluors or gold particles (Jackson et al., 1993; Wansink et al., 1993; Iborra et al., 1996). Alternatively, sites can be identified by immunolabelling polymerases, transcription factors, or the histone modifications associated with active chromatin (e.g. Grande et al., 1997; Pombo et al., 1999b; Muller et al., 2007), but then high concentrations may mark inactive components distant from polymerisation sites. Sites can also be localised using fluorescence in situ hybridisation (FISH) as they contain high local concentrations of nascent RNA (e.g. Femino et al., 1998). The general finding of these and other studies is that nascent transcripts copied from several different genes are concentrated in discrete sites known as 'factories' or 'active chromatin hubs' (Cook, 1999; de Laat and Grosveld, 2003; Chakalova et al., 2005; Misteli, 2007). Chromosome conformation capture (3C) and FISH confirm that transcription units lying far apart on the genetic map can nevertheless cluster into such factories – but only when active (Osborne et al., 2004; Simonis et al., 2006).

Despite the availability of these techniques, imaging nucleoplasmic sites remains difficult, largely because they are small enough to lie below the resolution of most light microscopes (Faro-Trindade and Cook, 2006b). Although resolution can be improved using special techniques (e.g. Martin et al., 2004), details are usually observed by electron microscopy (EM) (Pombo et al., 1999b; Wetterberg et al., 2001) – but then the stains used to increase contrast reduce resolution. Electron spectroscopic imaging (ESI) is a high-resolution and powerful ultrastructural method that has been used to map atomic distributions in unstained preparations; it has been applied to chromatin, interchromatin granule clusters (IGCs), promyelocytic leukaemia nuclear bodies, nucleoli, and sites where double-strand breaks are repaired (Bazett-Jones and Hendzel, 1999; Bazett-Jones et al., 1999; Eskiw et al., 2003; Eskiw et al., 2004; Dehghani et al., 2005; Politz et al., 2005; Kruhlak et al., 2006). We now apply ESI to map nucleoplasmic factories in HeLa cells at a hitherto inaccessible resolution; templates and nascent RNA are attached to enormous protein-rich structures with a characteristic atomic signature. We call these structures with their attached templates and transcripts 'factories', because the combination is large enough to contain both the nascent BrRNA used for identification, as well as many (or all) of the different proteins required to make a mature transcript (which include, for example, the machineries involved in capping, splicing, 3′ end formation, and nonsense-mediated decay). We do not suggest that all the machinery within these factories is active. Rather, we imagine that the minority is active, in much the same way that most RNA polymerase I in a nucleolar factory is an inactive store, with only a minority on the surface being engaged in transcription (Hozák et al., 1994). Nevertheless, the high local concentration of the majority will ensure efficient activity of the minority.

## Results

### ESI technique

We permeabilised HeLa cells in a 'physiological' buffer and allowed engaged polymerases to extend their transcripts by ~40 nucleotides in BrUTP (plus ATP, CTP, and GTP); after immunolabelling the resulting BrRNA with gold particles, phosphorus (P) and nitrogen (N) in 70-nm sections were mapped by ESI, and the structure of transcription sites (now marked by gold particles) analysed. Conditions used in vitro preserve nuclear structure and function (Jackson et al., 1988; Pombo et al., 1999b). For example, in optimal triphosphate concentrations, permeabilised cells initially synthesise DNA at in vivo rates. As the rate of RNA

synthesis in vivo is unknown, we could not determine the relative efficiency in vitro; however, we do know that tenfold more RNA than DNA is made, so RNA synthesis must also be efficient. Here, we used suboptimal triphosphate concentrations to limit elongation to ~40 nucleotides so few tagged transcripts can leave synthetic sites (Jackson et al., 1998).

In conventional EM, heavy elements such as uranium are used as stains to enhance contrast. An electron in the beam (blue) interacts with a positively charged atomic nucleus in the stain (brown) to be deflected from its path without energy loss (Fig. 1A). Fewer electrons then pass through a slit to hit the detector; these 'lost' electrons are equivalent in number to the blue area under the peak at 'zero loss', and – after printing – the image appears darker. In unstained areas, light atoms originally in the specimen (e.g. P) scatter few electrons, which pass straight through to give a lighter image. In ESI, sections are unstained, and contrast depends on endogenous atoms. Here, a beam electron (red) interacts with an electron orbiting a P nucleus (purple) to lose a characteristic amount of energy (i.e. 153 eV). It enters a spectrometer to be separated according to energy and used to create an energy-filtered image. Separation is partly achieved by repositioning the slit (centring at –155 eV selects electrons scattered from P). As background scattering falls off exponentially with –eV, the background (grey) under the red area can be calculated from the number of electrons deposited in a window centred at –120 eV. After printing, additional electrons in the red area give a brighter image – and a P map of the specimen. Beam electrons also interact inelastically with N atoms to lose 407 eV, and so can be mapped by repositioning the slit.

Fig. 1B illustrates a conventional EM image where nascent BrRNA has been immunogold labelled, and the section stained with uranyl acetate. Heterochromatin and the nucleolus are heavily stained to appear black-on-white (as uranium scatters electrons which fail to pass through the zero-loss window). Three gold particles (marking BrRNA) also scatter to appear dark against a rather featureless background (as the stain binds roughly equally to all regions; inset). By contrast, the P map (obtained by ESI) of a similar – but unstained section – shows heterochromatin as white-on-black, and detailed variations in P density are seen (Fig. 1C, left). Unpermeabilised cells yield similar P maps (Fig. 1C, compare left and right panels), so permeabilisation has little effect on gross morphology. As every residue in a nucleic acid contains one P atom – compared with the relatively few found in proteins – the P map mainly reflects the distribution of nucleic acid. [The C-terminal domain of the active catalytic subunit of polymerase II is one of the most highly phosphorylated protein domains (Kornberg, 2007), but even this subunit contains little P per residue when averaged over the whole.] We conservatively estimate that ESI applied to our sections is sufficiently sensitive to allow detection of only ~860 N atoms and ~50 P atoms (Materials and Methods). These values compare with the ~6200 N atoms in one molecule of RNA polymerase II and the ~8400 P atoms in its transcript (Jackson et al., 1998). Therefore, a single polymerase and its transcript can be detected easily.

## Nucleoplasmic sites are rich in nitrogen

Fig. 2 illustrates a typical transcription site imaged by ESI. In the zero-loss image (Fig. 2A), gold particles marking BrRNA appeared black against a featureless background. The P and N maps were complex (Fig. 2B,C), and white marked high concentrations of the respective atoms. We then prepared a triple merge, pseudo-colouring P red and N green, and inverting the grey-scale in the zero-loss image so gold particles (now white) could be seen more easily (Fig. 2D). They marked a N-rich structure (green) associated with chromatin (which yielded P and N signals of roughly equal intensity, and so appeared yellow). Such structures ('sites') marked by particles invariably appeared green (e.g. Fig. 2E-I) and so are rich in protein, even though they were identified by their content of (P-rich) BrRNA.

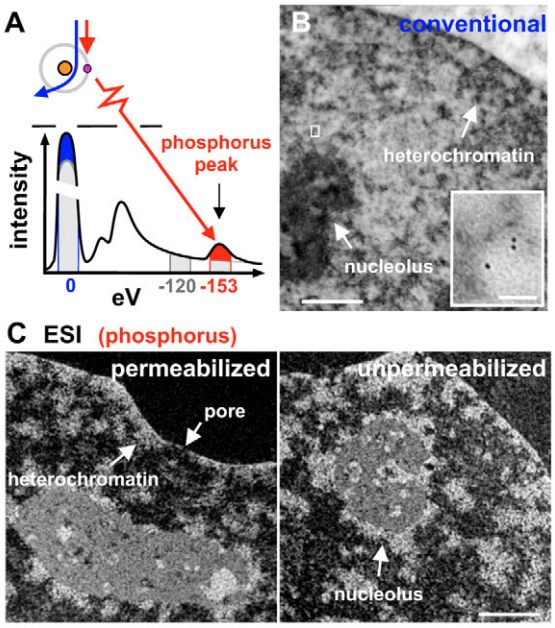


**Fig. 1.** Experimental approach. (A) Cartoon illustrating the principles that underly ESI. (B) Conventional EM image. HeLa cells were permeabilised, polymerases allowed to extend transcripts in BrUTP, BrRNA indirectly immunolabelled with gold particles, and 70 nm sections stained with uranyl acetate. The nucleolus and heterochromatin are heavily stained with the heavy metal, to appear black-on-white (as many electrons are scattered and so not detected). Inset, three gold particles (marking nascent BrRNA) also scatter electrons to appear dark. (C) ESI (P maps) of unstained cells (i.e. lacking uranyl acetate). Left, cell prepared as in B, but without staining. Right, control that was fixed directly, and was not permeabilised, immunolabelled or stained. P-rich structures, such as heterochromatin, appear white-on-black, and permeabilisation has little effect on morphology. Scale bars: 1 μm (inset in B, 50 nm).

## Defining nucleoplasmic transcription sites

We next confirmed that most gold particles mark (nascent) BrRNA, by extending transcripts in actinomycin D. Gold particles were categorised as lone or clustered, where a cluster is defined as two or more particles lying within 40 nm of each other. The transcriptional inhibitor reduced the number of both lone and clustered particles (Fig. 2J) – indicating that most particles marked nascent BrRNA. However, a few lone particles remained after drug treatment, so these represented the inevitable background. By contrast, no clusters were seen with actinomycin D, so all clusters must mark newly made BrRNA.

An initial survey of >150 clusters of gold particles seen in the absence of the drug revealed that 89% were associated with N-rich structures with diameters >40 nm (not shown). This suggests that most transcription sites are larger than 40 nm, as we would expect sectioning to generate the few smaller sites seen. Therefore, we only considered sites of >40 nm that were marked with clusters. This definition could bias selection towards larger sites, but three

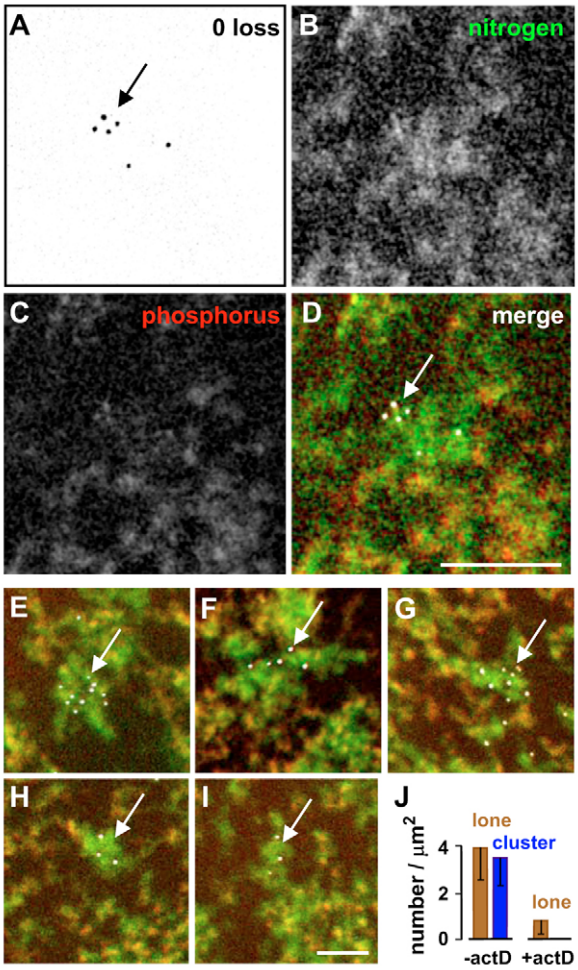


**Fig. 2.** Imaging sites (marked by BrRNA) using ESI. HeLa cells were permeabilised, nascent transcripts extended in BrUTP, cells fixed and BrRNA indirectly immunolabelled with gold particles; after sectioning (70 nm), elemental maps were collected by ESI. Arrows indicate clusters of particles. (A-D) Four views of one section. The zero-loss image reveals little other than the cluster of particles marking BrRNA, but P and N maps are complex; in the merge, the grey scale for the zero-loss image is inverted, and particles (now white) mark a N-rich structure. (E-I) Similar merges of other structures labelled with particles; all structures are N-rich. Scale bars: 100 nm. (J) After run-on ± actinomycin D, the number of lone (brown bars) and clustered particles (blue bars) in 15 images (total area 44 $\mu m^2$) as in D were counted; the inhibitor reduces the number of particles indicating that most mark nascent RNA. As a cluster typically contains 2.9 particles (123 sites analysed), the 2D density of sites marked by clusters is 1.2 sites/$\mu m^2$, which is equivalent to a 3D density of 10.3 sites/$\mu m^3$. Errors bars represent s.d.

arguments indicate any such bias is small. First, if it were large, we might expect single particles to mark smaller sites with less BrRNA; however, single and clustered particles marked sites with similar dimensions. For example, 63% of single particles are associated with N-rich structures of >40 nm (average diameter 89 nm), close to the expected maximum of 80% (as 20% remain after inhibition with actinomycin and represent background; Fig. 2J). Second, clusters of particles marked ~70% of all nucleoplasmic transcription sites, as we detected ~10.3 sites/$\mu m^3$ (Fig. 2J, legend) compared with the 14.7 sites/$\mu m^3$ found when all sites are detected using cryosections that permit more efficient immunolabelling (Pombo et al., 1999b). We did not use cryosections for this analysis as they are stabilised with a resin that is incompatible with N mapping. Third, and perhaps most decisively – sites were normally distributed about a mean of 87 nm, with few between 40-60 nm in diameter (below) and fewer still <40 nm.

Perimeters around N-rich structures (which may or may not be marked by clusters) were drawn using the approach illustrated in Fig. 3A-D. First, the intensity in each pixel in a P map (Fig. 3B) was subtracted from its counterpart in the N map (Fig. 4A); this process is equivalent to removing chromatin from the image, as nucleosomes yield similar intensities in both channels (Table 1). The resulting image was then binarised, and any holes within N-rich structures filled; this generated a few large (solid) structures and many small (solid) ones. One pixel around all structures was then removed ('eroded'), and the process repeated; many small structures disappeared. Next, remaining structures were restored to their original size by adding (twice) one pixel to the outside (i.e. by 'dilation'). Structures with diameters >40 nm were then selected, which is justifiable because all clusters were associated with N-rich structures of >40 nm (above). Only three structures coloured purple, blue, and orange remained in this case (Fig. 3C). These three structures were used as 'masks' which are placed over the corresponding positions in the zero-loss/P/N merge, and used to identify the three structures illustrated in Fig. 3D. The orange mask covered a site that is transcriptionally active as it was marked by three gold particles. The purple mask could cover another site because it possessed the appropriate P:N ratio (not shown), but it was unlabelled; therefore, we cannot be certain that it was transcriptionally active. The blue mask could not cover a transcription site, as it had an inappropriate P:N ratio (not shown). [Its P:N ratio is typical of a coiled body (not shown).] We used masks prepared in this way to define precisely perimeters around sites of >40 nm that were also marked by clusters of gold particles. Such perimeters excluded abutting P-rich regions that may well contain associated templates and transcripts; therefore, complete sites will be even larger than the cores measured here. Perimeters defined in this way inevitably differ from those that we have mapped previously using just the clusters of gold particles (see Pombo et al., 1999b).

### Diameter of transcription sites

Transcription sites were selected by first choosing clusters, and then drawing perimeters around any N-rich cores (as in Fig. 3A-D). Sixty-nine clusters were selected at random; all were associated with N-rich cores of >40 nm (i.e. at least one particle in the cluster lay within the perimeter around a N-rich structure). The average diameter – determined assuming cores were spheres (justified in Materials and Methods) – was 96 nm (Fig. 3E, black bars). As this is greater than section thickness, many sites were cut during sectioning to lose polar caps, whereas others were present only as caps. After correcting for the 'Holmes' effect, we found true diameters to be normally distributed (Materials and Methods) about a mean of 87 nm, with ~75% lying between 60-120 nm (Fig. 3E, grey bars). Importantly, few sites had diameters of 40-60 nm, so even fewer can be <40 nm and so missed; this indicates that there are unlikely to be many transcription sites of <40 nm.

### Phosphorus and nitrogen content of transcription sites

The number of P and N atoms in sites was determined by reference to the core nucleosome (with 146 bp DNA), which has a known atomic constitution (Luger et al., 1997; Bazett-Jones et al., 1999). To establish the accuracy of our approach, we estimated numbers

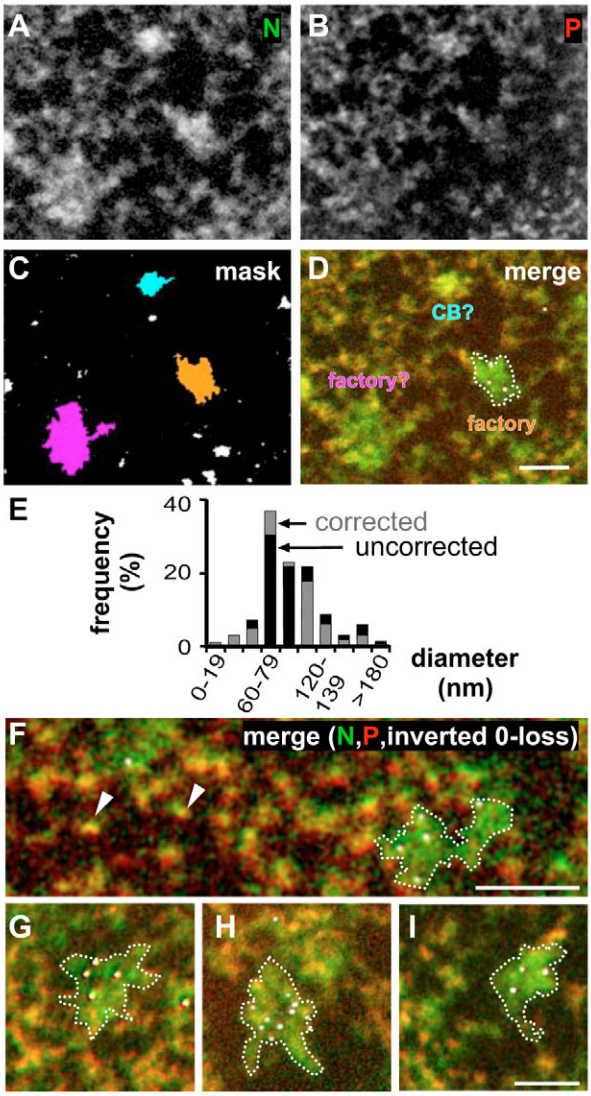


**Fig. 3.** Site perimeter, diameter and atomic content. (A-D) Perimeters of N-rich structures are mapped by subtracting the intensity in each pixel (1.35 $nm^2$) in a P map (B) from its counterpart in the N map (A); this process is equivalent to removing chromatin from the image (as nucleosomes yield similar intensities in both channels; Table 1). Next, the resulting image is binarised, holes within (N-rich) structures filled, structures 'eroded' by 1 pixel (1.35 $nm^2$) twice (to remove small structures), and then 'dilated' twice to restore structures to the original size. The resulting masks (C) outline various structures; those with diameters >40 nm were selected (justifiable because all clusters are associated with N-rich structures of >40 nm). The three remaining structures are coloured purple, blue, and orange, and their perimeters are overlaid over the zero-loss/P/N merge (D). One perimeter bounds an active transcription site marked by three particles, another (purple) could ring a site (it possesses the appropriate N:P ratio) but is not labelled with gold, whereas a third (blue) cannot be a site (it has the N:P ratio of a coiled body; not shown).
(E) Frequency of site diameters. Sites were selected by choosing those marked by clusters, and then drawing perimeters around associated N-rich structures ($n$=69) as in D. Major and minor (orthoganol) axes of structures were measured, and diameters calculated (assuming underlying structures are spheres) and binned (20-nm bins of 0-19, 20-39, 40-59 nm, etc.). Diameters were corrected for effects of sectioning, which can remove polar caps (such correction gives rise to sites of <40 nm). Uncorrected and corrected diameters were normally distributed (Materials and Methods) about means of 96 and 87 nm, respectively. If many small sites were being missed, the distribution would be highly skewed to the left with many more 40-60 nm structures being seen.
(F-I) N and P content were determined using merges such as that in D with nucleosomes (arrowheads) as references. Dotted lines: perimeters of N-rich structures marked by gold particles. Scale bars: 100 nm.

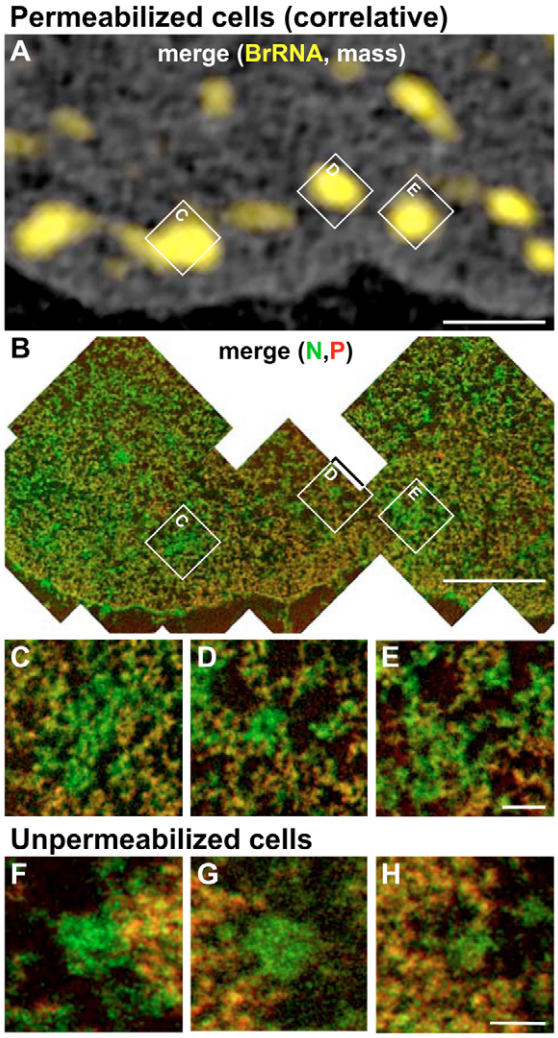


**Fig. 4.** Identifying sites by correlative microscopy and in unpermeabilised cells. (A-E) Permeabilised HeLa cells were allowed to extend nascent transcripts in BrUTP, and the resulting BrRNA indirectly immunolabelled with Cy3; cells were then embedded, sectioned (70 nm), and images of the same sections collected by fluorescence and electron microscopy. (A) Merge of fluorescence and –155 eV EM images; sites containing nascent BrRNA (yellow) are scattered throughout the nucleoplasm (grey). Insets, selected areas shown in B-E. (B) Collage of ESI merges (P, red; N, green) of the same region. (C-E) Typical ESI merges (P, red; N, green) of regions shown in insets in A and B. (F-H) Cells were directly fixed, sectioned (without immunolabelling), P and N maps collected and merged, perimeters around N-rich regions mapped (as in Fig. 3C), and nucleoplasmic structures with diameters and P:N ratios typical of active transcription sites (i.e. >40 nm and 0.38±0.1) selected; three examples are shown. These sites by definition have similar diameters and P:N ratios to their labelled counterparts in permeabilised cells; they also have similar textures. Scale bars: 1 μm (A,B); 100 nm (C-H).

in a (cytoplasmic) ribosome, which is known to contain ~6880 P atoms (Materials and Methods) and which we have previously used as a reference (Iborra et al., 2000). Circles of appropriate diameter (i.e. 11 and 22 nm for nucleosome and ribosome, respectively) were placed over the structures, and relative numbers calculated by simple proportion; despite the use of such a crude approach, we reassuringly found roughly half the expected number of P atoms in a ribosome (Materials and Methods).

We next estimated atomic numbers within perimeters around N-rich structures marked by clusters (Fig. 3F). Despite the variety of

structures seen (e.g. Fig. 3F-I), the standard deviation of P:N ratios was small (Table 1). Sites contained surprisingly little P; if all P was contained in nucleic acid, there would be sufficient for only ~4800 nucleotides. Even so, sites were enormous, with a mass of ~10 MDa – which is equivalent to the mass of ~28 core polymerase molecules (Table 1).

### Identifying transcription sites in unpermeabilised cells and by correlative microscopy

As gold particles can obscure underlying structures, we identified sites by immunofluorescence before analysing the ultrastructure of the same sites by EM. Patience and skill are needed for such 'correlative microscopy' (e.g. Pombo et al., 1999a), but improvements now make it somewhat easier (Ren et al., 2003). Nascent BrRNA was immunolabelled with Cy3, and superimposition of a fluorescence image of a section on the low-magnification EM image gave a merge in which yellow foci marked BrRNA (Fig. 4A). Relevant areas containing foci (boxes) were then identified in a collage of medium-power P/N merges of the same area (Fig. 4B) before details were analysed at high magnification (Fig. 4C-E). Fluorescent foci and N-rich structures were found in the same area, and the latter had diameters and P:N ratios similar to those marked by clusters of gold particles (Table 1).

We also confirmed that sites with similar diameters and P:N ratios could be detected in unpermeabilised cells. Cells were fixed directly, sectioned (without immunolabelling), and ESI images collected. After mapping perimeters around N-rich regions as in Fig. 3C, nucleoplasmic structures with a P:N ratio typical of sites (i.e. 0.38±0.1; Table 1) were selected (Fig. 4F-H). Of 14 structures analysed, 13 had diameters between 60 and 120 nm, with one of 160 nm (Table 1); this is typical of active sites identified by immunogold labelling (Fig. 3E). Although we cannot formally prove that these are transcriptionally active, they had the appropriate size and atomic signature.

### Some properties of transcription sites and their environs

To compare mass densities, we analysed various other nuclear structures; sites were one-tenth as dense as nucleosomes, but more dense than the granular component (GC) of the nucleolus, IGCs, and chromatin (Table 1; the footnote to Table 1 indicates that the values we obtained for these structures were close to those found previously). This means that sites cannot be completely packed with protein, presumably because large invaginations extend from the surface into the interior (which is clearly suggested by inspection of Figs 3-5) and/or the interior is porous (i.e. sponge-like).

We next analysed some other properties of sites and their environs, and some additional examples are illustrated in Fig. 5. To gauge the significance of the property under consideration, we compared 44 true sites (i.e. labelled with ⩾2 gold particles, or identified by correlative microscopy) and 58 'virtual' sites (selected by placing circles of equivalent size at random on 12 images). (1) True sites were often surrounded by a space free of P and N (Fig.

**Table 1. Properties of nucleosomes and transcription sites**

| | | Transcription site | | |
|---|---|---|---|---|
| Property | Nucleosome | Immunogold | Correlative | Unpermeabilised |
| Diameter (nm) | | | | |
| Uncorrected | 11 | 96±31 | 103±22 | 109±26 |
| Corrected* | 11 | 87 | 94 | 102 |
| P:N ratio† | 1.0±0.1 | 0.38±0.12 | 0.26±0.07 | 0.38±0.07 |
| Number of atoms‡ | | | | |
| P | 292 | 4800 | 6500 | 8700 |
| N | 2605 | 198,000‡ | 204,000 | 208,000 |
| Equivalents§ | | | | |
| Nucleosome (P) | 1 | 17 | 22 | 30 |
| Nucleosome (N) | 1 | 75 | 115 | 113 |
| Polymerase II (N) | 0.4 | 28 | 28 | 27 |
| Mass (MDa)§ | | | | |
| Nucleic acid | 0.10 | 1.7 | 2.1 | 3.0 |
| Protein | 0.11 | 8.3 | 12.7 | 12.4 |
| Total | 0.21 | 10 | 15 | 15.4 |
| Density§ | | | | |
| P atoms/nm$^3$ | 0.42 | 0.14 | 0.15 | 0.16 |
| N atoms/nm$^3$ | 3.8 | 0.57 | 0.47 | 0.38 |
| Da/nm$^3$ | 300 | 29 | 34 | 28 |

| Property | Chromatin | GC | IGC |
|---|---|---|---|
| P:N ratio† | 1.0±0.1 | 0.8±0.1 | 0.5±0.07 |
| Density§ | | | |
| P atoms/nm$^3$ | 0.03 | 0.025 | 0.029 |
| N atoms/nm$^3$ | 0.17 | 0.27 | 0.24 |
| Da/nm$^3$ | 17 | 20 | 20 |

Values are means (±s.d.) obtained for ⩾330 nucleosomes, and 55, 10 and 14 sites detected by immunogold labelling (e.g. Fig. 4), correlative microscopy (e.g. Fig. 5A-E) or in unpermeabilised cells (e.g. Fig. 5F-H), respectively. See Materials and Methods for procedures and assumptions.

*Corrected for 'Holmes' effect.

†Ratio of intensity (arbitrary units/pixel) after subtracting background in resin. Politz et al. (Politz et al., 2005) used ESI and nucleosomes as references to obtain P:N ratios in atoms of 0.13 (chromatin) and 0.08 (GC); these compare with our values (not shown) of 0.14 (chromatin), 0.09 (GC), and 0.12 (IGC).

‡Values for sites calculated from the area and average P or N intensity/pixel compared with nucleosome, corrected for the loss of polar caps that occurs when an 87 nm sphere is placed centrally in a 70 nm section.

§From relative number of atoms.

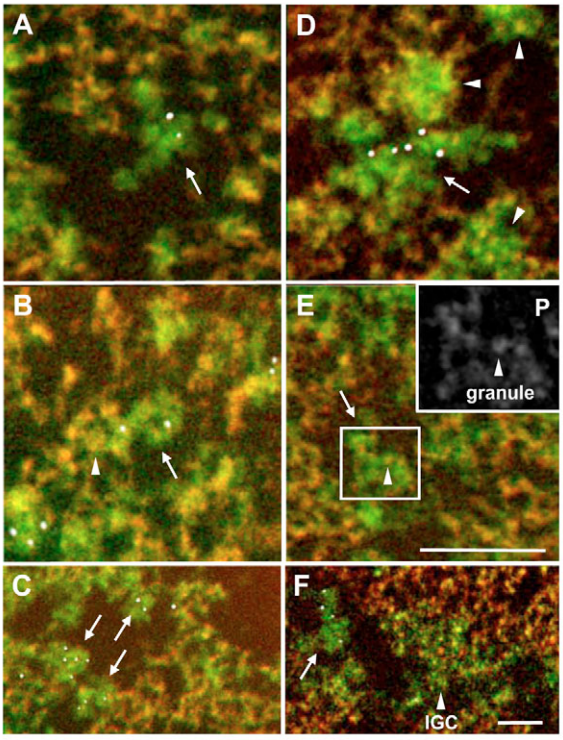


**Fig. 5.** Site morphology. Merges were prepared as in Fig. 3D (A-D,F) and Fig. 4C (E). Arrows indicate transcription sites marked by gold particles. (A) Site marked by two gold particles surrounded by space free of P and N. (B) Site marked by particles surrounded by chromatin (arrowhead marks RNPs and/or nucleosomes). (C) Three sites marked by particles lying close to each other. (D) Site marked by particles lying near other gold-free structures (arrowheads) that have dimensions and P:N ratios typical of sites. (E) Site containing many P-rich granules (arrowhead) smaller than nucleosomes. This site was selected by correlative microscopy because there are no obscuring gold particles (but similar granules are seen by immunogold labelling). Inset, P map. (F) Site lying near IGC (arrowhead). Scale bars: 100 nm (A,B,D,E); 50 nm (C,F).

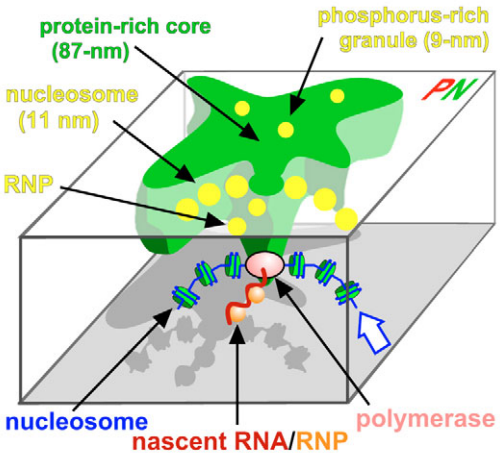


**Fig. 6.** Cartoon illustrating a section through a site. An active polymerase (attached to a core) reels in its template (blue arrow) as it extrudes its transcript; only one of ~eight polymerising complexes on the surface is shown. The upper face of the section illustrates how this structure appears in an ESI merge. The N-rich core appears green, except for several (yellow) granules that each contain ~70 P atoms; nucleosomes and RNPs (both yellow) are found on/near the surface. Sectioning often removes one or other pole with any associated templates/transcripts, while leaving those tethered to equators. When viewed from above, most RNA is then seen associated with equators, with little apparently lying within cores (see Materials and Methods for quantitative analysis).

5A). This property was significant; 87% sites were surrounded by at least one quadrant (extending 25 nm away from the surface) that contained no P or N, compared with the 53% obtained randomly ($P$=0.002; Fisher's $t$-test). This finding that there was a lot of empty space within nuclei contrasts with old ideas that nuclei are tightly packed with chromatin; however, we now know that ~70% nuclear space is not occupied by chromatin, nucleoli, or the various nuclear bodies – even in unpermeabilised cells (e.g. Dehghani et al., 2005). This finding is also consistent with transcription occurring in more 'open' regions of chromatin. (2) 76% of true sites had at least one such quadrant containing chromatin fibres and/or RNP granules (as in Fig. 5B); this is similar to the 75% seen with virtual sites and so is not significant. In other words, the high value arises simply because there are so many nucleosomes in the nucleus. (3) 77% of true sites also lay within 200 nm of another site as in Fig. 5C, significantly more than the 31% obtained with virtual sites ($P$<0.001). (4) Some labelled sites also lay near other structures with diameters and P:N ratios indicative of transcription sites but which are not labelled with gold (Fig. 5D). (5) 83% of true sites also contained 3-5 P-rich granules (diameters 8.9±1.7 nm) apparently distributed throughout the cores as in Fig. 5E. These are too small to be nucleosomes; they are also less dense (i.e. 45%), and contain only ~70 P atoms (not shown). (6) As nascent RNA was originally seen at the edge of heterochromatin (Fakan, 2004), we checked to see whether true sites also lay near dense chromatin but saw no such bias. There is also no clear demarcation between euchromatin and heterochromatin; rather P-density varies continuously (not shown) – consistent with previously reported results using other methods (Sadoni and Zink, 2004; Faro-Trandade and Cook, 2006a). (7) Analysis of low-magnification images also showed that 25% of true sites lay within 200 nm of IGCs (Fig. 5F), but ICGs are sufficiently numerous that a similar juxtaposition was seen with the virtual sites.

## Discussion

### Advantages and disadvantages of ESI

We used ESI to map nucleoplasmic transcription sites at an unprecedented resolution; this technique is sensitive enough to detect a single polymerase and its transcript under our conditions (Materials and Methods). Transcripts in permeabilised HeLa cells were extended in BrUTP by ~40 nucleotides, and the resulting BrRNA immunolabelled with 5 nm gold particles; using 70 nm sections and nucleosomes as internal references, we found BrRNA invariably associated with polymorphic N-rich (but P-poor) structures of ~10 MDa and ~87 nm in diameter (Table 1). Although heterogeneous in shape, these structures are surprisingly uniform in diameter and mass (Table 1).

As with all approaches, ours has both advantages and disadvantages: (1) Although sites were detected using the best available marker – polymerising activity – material may be lost and/or structure distorted during permeabilisation; however, we used conditions that preserve activity and morphology to the greatest extent possible (Fig. 1C,D) (Jackson et al., 1988; Pombo et al., 1999b). Perimeters around the structures were also defined using an algorithm (Fig. 3A-D) that eliminates most observer-based bias, and this probably underlies the remarkable uniformity seen in the

properties of such polymorphic sites (Table 1). We are also fortunate that few – if any – other nuclear structures have the same P:N ratio, so that this characteristic atomic signature can be used to identify similar structures in unpermeabilised cells (Table 1). Note, however, we cannot be certain such structures are transcriptionally active, in the absence of a suitable label. (2) Cutting sections thinner than the structure analysed removes material; nevertheless, some lost information can be recovered using stereological techniques. (3) Gold particles obscure underlying structures; therefore, results were confirmed by correlative microscopy (Fig. 4A-E). (4) Immunolabelling antibodies will add extra protein, leading to an overestimate of protein content. Fortunately, this effect is likely to be small, because even if each of the three particles that typically mark a site are associated with six immunoglobulin G molecules, the added protein would still constitute only ~15% of the total (Table 1). Moreover, it is unlikely that antibodies add much extra protein to the nascent BrRNA, as sites with essentially the same diameters and P:N signatures are seen in unpermeabilised cells that have never been immunolabelled – and so cannot be associated with antibodies (Fig. 4F-H; Table 1). (5) Selection of sites of >40 nm may bias analysis towards larger sites, but various arguments indicate that if there is such bias it is also small (Results). For example, site diameters are distributed about a mean of 87 nm, with few having diameters as small as 40-60 nm (Fig. 3E); if sites are distributed normally (which the evidence indicates), fewer still will be less than 40 nm. (6) Technical shortcomings prevent detection of all sites, but we nevertheless saw ~70% of them; therefore, the majority of sites are analysed. Despite these disadvantages, we hope these results confirm that ESI is a useful additional method to analyse structures of ~100 nm that lie within the 'resolution gap' (i.e. below the limit of resolution of the optical microscope, but well above that of conventional EM).

As quantitative ESI is a largely untried technique (at least when applied to biological specimens), we checked that it could be used to count the number of P atoms in another structure with a known number of atoms – the ribosome. Using nucleosomes as references, we found that we underestimate the number of P atoms in ribosomes by ~50%. Therefore, the values presented in Table 1 probably underestimate the measured numbers of P atoms by about half. We also assume sites contain RNA polymerase II, but one-fifth will contain the minor nucleoplasmic enzyme polymerase III (Pombo et al., 1999b).

### Properties of transcription sites

Sites contained a protein-rich core of ~87 nm; this is slightly larger than just the BrRNA or polymerase II associated with such sites (e.g. Pombo et al., 1999b; Martin et al., 2004) (reviewed by Faro-Trindade and Cook, 2006b). This core is one-tenth as dense as a nucleosome, and twice as dense as chromatin (Table 1). Clearly, sites cannot be completely packed with protein (as in a nucleosome), presumably because large invaginations extend from the surface into a more solid body (Figs 3-5) and/or the body is porous like a sponge. We can only speculate as to which proteins the body might contain. One obvious candidate is the polymerase. We note one crystalline form of the elongation complex of polymerase II contains 8 sets of the 12-subunit polymerase per unit cell; this organisation is very open [i.e. ~80% solvent (Kettenberger and Cramer, 2006)], and has a density of N atoms only ~fourfold higher than the core of the transcription site. Additional candidates would include some or all of the many different proteins involved in making a mature transcript (e.g. those involved in capping, splicing, 3′ end formation and nonsense-mediated decay). Much of this machinery may well be inactive, but the high local concentration of the majority will ensure efficient activity of the minority.

The 87-nm core contains only ~4800 P atoms (Table 1); this is roughly half the number in only one of the ~8 nascent transcripts (each with ~8,400 nucleotides) typically found in a transcription site (Jackson et al., 1998; Faro-Trindade and Cook; Marenduzzo et al., 2006). Much of what little P there is can be found in 9 nm granules, which are too small to be nucleosomes (Fig. 5E), and again we can only guess as to what these might be. Candidates include the individual granules seen in perichromatin fibrils (Fakan, 2004) and those in the ~40 nm particles associated with Balbiani rings (Olins et al., 1992). This paucity of phosphorus suggests that both nascent RNA and templates must lie outside cores, presumably attached to the surface. Two elements in our approach would then combine to ensure that so little phosphorus is seen in the cores. First, we exclude nucleosome-rich regions when defining core perimeters (Fig. 3A-D); RNP-rich regions are also probably excluded as we would expect them to have a similar N:P ratio. Second, cutting 70 nm sections through ~87-nm cores (with attached transcripts and templates) will inevitably remove most material attached to the poles of those cores, but it will leave most attached to the equators; then, when viewed from above, most phosphorus in transcripts and templates will be seen lying around cores, with little apparently lying within (as is the case). See Materials and Methods for a more complete discussion of these effects of sectioning.

We conclude that a complete transcription site is an enormous structure composed of an ~87 nm (porous) core with active polymerases (plus templates, transcripts) attached to the surface (Fig. 6). This is an attractive organisation; we assume that the surface can be accessed easily, and there is sufficient space on it to accommodate simultaneously many of the diverse set of components required to make a transcript (e.g. there is space to pack ~160 polymerising complexes of 15 nm). Attachment to such a large structure also helps explain why treating permeabilised cells with nucleases detaches few (if any) active polymerases, or their templates and transcripts (reviewed by Marenduzzo et al., 2007).

### Relationship of site structure to models for transcription

In the traditional model for transcription, a single polymerase diffuses to its target promoter before tracking along the template as it makes RNA. It would then have to drag along this enormous complex as it did so. It seems more probable that the polymerase is immobilised on the surface of the core, where it reels in its template as it extrudes its transcript (Fig. 6) (Cook, 1999). Alternatively, one template might be transcribed by several polymerases attached to one core, but it again seems more likely that a string of enzymes on the surface reels in the one template. Results are also consistent with a possibility in which ~eight polymerases active on different templates are bound to the surface of the core. Support for this comes from several sources (Faro-Trindade and Cook, 2006b; Marenduzzo et al., 2007). First, there are ~eightfold more active molecules of RNA polymerase II than factories, and – as only one polymerase is typically engaged per transcription unit – each factory would transcribe ~eight different units. Second, 3C and FISH show sequences lying far apart on the genetic map can nevertheless lie close together in 3D space, and, significantly, contacting sequences are usually transcriptionally active (e.g. Osborne et al., 2004; Simonis et al., 2006); this means that in these cases the relevant factories must contain at least two

active units. If this last possibility applies, nucleoplasmic and nucleolar sites would then have the same general structure, with active polymerases transcribing several different units on the surface of a supporting core (Hozák et al., 1994). One challenge now is to relate the structures seen with ESI to those seen previously by the traditional approach – for example, of individual polymerases (Wetterberg et al., 2001) and perichromatin fibrils (Fakan, 2004) – and to obtain higher-resolution maps of polymerases (and all the additional machinery required to make a mature transcript) in and around these factories.

## Materials and Methods

### Cell culture and nuclear run-ons

HeLa cells were grown in DMEM high glucose media (BRL-Gibco, Paisley, UK) with 10% foetal calf serum (BRL-Gibco), plated on 25 mm glass coverslips (number 1.5; Agar Scientific, Stansted, UK), regrown to 90% confluency, and washed in ice-cold PBF. PB ('physiological' buffer; pH 7.4) is 100 mM potassium acetate, 40 mM KCl, 10 mM $Na_2HPO_4$, 1 mM $MgCl_2$, 1 mM $Na_2ATP$, 1 mM dithiothreitol, plus RNase inhibitors (Sigma-Aldrich, Poole, UK); PBF is PB plus 50 mg/ml Ficoll 70 (Sigma). Cells were then permeabilised (5 minutes; 4°C) in PBF plus 50 μg/ml saponin (Sigma), washed quickly in PBF to remove endogenous nucleotides, incubated (15 minutes; 33°C) in PBF containing 100 μM ATP, CTP and GTP (Roche Scientific, East Sussex, UK) plus 100 μM BrUTP (Sigma), and fixed (10 min; 20°C) in 4% paraformaldehyde in 155 mM HEPES (pH 7).

### Immunolabelling BrRNA and embedding

After fixation, cells were permeabilised (5 minutes; 20°C) with 0.5% Triton X-100 in PBS, washed and blocked (1 hour) in 1% BSA (Sigma) in PBS. BrRNA was indirectly immunolabelled by incubation (3 hours at 20°C, or 16 hours at 4°C) in 1% BSA in PBS plus mouse anti-BrdU (1:1000 dilution; catalogue number PRB1U, Phoenix Flow Systems, San Diego, CA; or catalogue number sc-32323, Santa Cruz Biotechnologies, Santa Cruz, CA), washing three times (30 minutes) in 1% BSA in PBS, and incubation with goat anti-mouse conjugated with 5 nm gold particles (1:50 dilution; incubation for >24 hours at 4°C to ensure penetration; British BioCell, sold by Agar Scientific, Stansted, UK) or with donkey anti-mouse conjugated with Cy3 (1:500 dilution; incubation for 2 hours at 20°C; Jackson ImmunoResearch Labs, West Grove, PA). After washing (30 minutes) three times with 1% BSA in PBS, cells were fixed (10 minutes) in 1% glutaraldehyde, dehydrated (30 minute steps with gentle shaking) through 30, 50, 70 and 90% ethanol, washed (30 minutes) three times in 100% ethanol, infiltrated (2 hours with gentle shaking) successively with Quetol 651 (Agar Scientific) twice and then with Quetol 651 containing 2% hardener (DMP-30; Agar Scientific), and transferred to fresh Quetol 651 with hardener to cure (70°C; 16 hours).

### Electron spectroscopic imaging and correlative microscopy

Sections (70 nm) were collected on 300 mesh copper grids (Agar Scientific). For EM, sections were carbon coated by glow discharge, and ESI maps collected (Bazett-Jones and Hendzel, 1999; Bazett-Jones et al., 1999) using a Zeiss/LEO 912 (with in-column omega filter, Zeiss 2048×2048 pixel camera; 'AnalySIS' v4 (Soft Imaging Systems, Helperby, UK), emission voltage 80 keV), or FEI Tecnai 20 (with post-column Gatan imaging filter, 1024×1024 pixel camera, Digital Micrograph software (Gatan, Warrendale, PA), emission voltage 200 keV). Both EMs had stages cooled with liquid nitrogen. For P maps, images of a region were collected in windows centred at –120 and –155 eV (slit-widths 20 eV), and background in the –155 eV window (determined using the 'two-window exponential method') subtracted to give the net P image. For N maps, images were collected using windows centred at –385 and –415 eV and treated similarly. Zero-loss images were also collected. For correlative microscopy (Ren et al., 2003), fluorescence micrographs were collected using a Zeiss Axioplan equipped with an AxioCam CCD camera (Welwyn Garden City, UK) and a 63× objective (numerical aperture 1.4); EM images were collected as above. Images were analysed using 'Image J' (Rasband, 1997-2007) and 'iTEM' (Soft Imaging Systems), and false coloured using Adobe 'Photoshop' v9 (Uxbridge, UK). Background measured in areas in the same section that lacked cells was subtracted from each pixel. Images were prepared for presentation (but not for analysis) using a two-pixel Gaussian blur to remove noisy pixels.

Errors arise during quantitative ESI from several causes. Thus, at 16,000× magnification and 1.6 mrad dose, it takes 2×100 seconds and 2×20 seconds to collect information in the two N and P windows, respectively. Then, some specimen drift and mass loss can occur; however, the former is easily recognised, because gold particles and nucleosomes appear blurred (and then images were not used), and the latter does not affect calculation of atom numbers (because nucleosomes in the same specimen serve as internal references). Small errors also arise from background subtraction. Thus, background in an area the size of a nucleosome (i.e. 97 $nm^2$) was 6±3% and 11±4% of the respective P and N (uncorrected) signals seen in a nucleosome. Another error can arise from variations (±10%) in section thickness.

### P and N content

For Table 1, the number of P and N atoms in a site was determined by reference to numbers calculated for a nucleosome, which is assumed to be 11 nm in diameter and to contain 146 bp DNA (42% GC) plus two unmodified copies of each of the four core histones (HIST2H2AA, HIST2H2BE, HIST1H3A, HIST1H4A), and so 292 P plus 2605 N atoms. Of the N atoms, 1083 are in DNA and 1522 in protein; for every P atom, there are 3.7 (i.e. 1083/292) N atoms in nucleic acid. In each pair of ESI maps, average P and N intensities/pixel in 11 nm circles (area 97 $nm^2$) centred on 6-10 lone nucleosomes were determined, and intensity units/pixel related to number of atoms. Total numbers of P and N atoms in a site in the same image were calculated by proportion; values were then converted to nucleosome equivalents. The mass of nucleic acid and protein in a site was determined assuming all P is in nucleic acid, that each P atom is associated with 3.7 N atoms in nucleic acid (as in a nucleosome), and that the rest of the N is in protein. We also assumed the polymerase II core complex contains 1 copy of POLR2A-L (RPB1-12) and so 6226 N atoms. When checking the accuracy of our experimental estimate of the number of P atoms in a ribosome, we assumed a ribosome (diameter 20 nm) contained 6,880 nucleotides of ribosomal RNA (i.e. 4700, 1900, 160 and 120 nucleotides in 28S, 18S, 5.8S and 5S rRNAs) – and so P atoms. Using phosphorus images of unpermeabilised cells, 20 nm and 11 nm circles were placed over 106 (cytoplasmic) ribosomes and 90 nucleosomes, respectively, in nine images, and intensities of P and N measured. Background intensities in cell-free areas were subtracted, and the number of P atoms in a ribosome calculated. The ribosome:nucleosome ratio of intensities/circle was 9.5±3.5:1. If we assume the core nucleosome contains 146 bp DNA (and so 292 P atoms), we estimate experimentally that a ribosome contains ~2900 P atoms, or ~42% of the expected number. If the nucleosome contains linker DNA (and so 400 P atoms), our estimate rises to 57%.

We estimated (conservatively) the limits of detection of P and N as follows. If (1) a core nucleosome contains 292 P atoms and 2,605 N atoms (above), (2) background in an area the size of a nucleosome is 6 and 11% of the respective P and N signals (above), and (3) true signal is at least threefold higher than the background, then we should be able to detect structures containing ~50 P atoms and ~860 N atoms. These values compare with the ~8400 P atoms in a typical nascent transcript (Jackson et al., 1998), and the 6226 N atoms in RNA polymerase II.

### Site diameter and effects of sectioning

Standard stereological procedures were used (Williams, 1977). The diameter $d$ of a site was determined by measurement of the major $x$ and minor $y$ (orthoganol) axes of each site in an image, from $d=\sqrt{(xy)}$. This assumes sites are spherical, which can be justified because the aspect ratio ($x/y$) is 1.49, and treating an ellipsoid with this aspect ratio as a sphere introduces <3% error in diameter (Weibel, 1979). The average diameter in the population was then determined using Fullman's formula, and corrected for the 'Holmes' effect using the sequential-subtraction method (Weibel, 1979; Pombo et al., 1999b). This allows the diameter $D$ of spheres to be deduced from diameters ($d$) of circular profiles seen in 2D images of 3D sections cut through the sample. Spheres lying completely in sections appear as circles with diameter $D$; any cut nonequatorially may give polar caps that either appear smaller, or are missed because they are too small to be detected. The distribution coefficient $K$ was 1.15, indicating the distribution of diameters seen was close to normal (Weibel, 1979). The number of sites in the three dimensions of the nucleoplasm was calculated from the density seen in the two dimensions of a section using Abercrombie's formula (Pombo et al., 1999b). The minimum sample size was estimated using the progressive mean; for immunogold labelling in Table 1, the last 30 values analysed lay within 5% of this mean.

The effects of sectioning can generate apparently paradoxical results. In discussing these, we assumed that immunolabelling particles mark exactly where BrRNA is, even though they can lie up to ~20 nm away because of the dimensions of the antibodies involved (e.g. Iborra and Cook, 1998). One paradox is: if BrRNA is on the surface, why do gold particles apparently lie within factories? Geometric considerations indicate that cutting 70 nm sections through 87 nm cores results in ~89% cores retaining one or other pole. When viewed from above, particles marking BrRNA at the remaining pole then appear to lie within a core. A related paradox is: why do we see so little internal P, when these particles mark RNA, which we know contains P, and when P-rich templates must also be present? The answer partly depends on our exclusion of P-rich regions when defining perimeters (Fig. 3A-D), and partly from sectioning. Only the last ~40 of the ~8400 nucleotides in a growing transcript are labelled with bromine; as a result, sectioning will often remove the bulk of the transcript (with its P atoms) from the terminal ~40 nucleotides with its bromines that is attached to the surface of the core. Thus, if the centre of mass of a transcript lies 25 nm immediately above or below its polymerising site at a pole (a conservative estimate as a polymerase and RNP particle are ~15 and 10 nm, respectively), if a core can only be detected when at least one-third of its BrRNA (and so surface) is retained, and if the immunolabelling particle is found immediately at the pole, geometric considerations indicate that only one-third of cores will retain both the particle and centre of mass. Sectioning will similarly detach much of any template tethered to a pole. Of course, transcripts and templates tethered to equators will usually be retained in sections, and this is where most associated P is seen.

We thank the E. P. Abraham Research Trust, the Biotechnology and Biological Sciences Research Council, the Marie Curie Fund of the European Union (MEIF-CT-2005-023821), and the Wellcome Trust for support; we also thank Mike Shaw, and especially David Bazett-Jones for allowing us to collect some of the images on his microscope.

## References

**Bazett-Jones, D. P. and Hendzel, M. J.** (1999). Electron spectroscopic imaging of chromatin. *Methods* **17**, 188-200.

**Bazett-Jones, D. P., Hendzel, M. J. and Kruhlak, M. J.** (1999). Stoichiometric analysis of protein- and nucleic acid-based structures in the cell nucleus. *Micron* **30**, 151-157.

**Chakalova, L., Debrand, E., Mitchell, J. A., Osborne, C. S. and Fraser, P.** (2005). Replication and transcription: shaping the landscape of the genome. *Nat. Rev. Genet*. **6**, 669-677.

**Cook, P. R.** (1999). The organization of replication and transcription. *Science* **284**, 1790-1795.

**Dehghani, H., Dellaire, G. and Bazett-Jones, D. P.** (2005). Organization of chromatin in the interphase mammalian cell. *Micron* **36**, 95-108.

**de Laat, W. and Grosveld, F.** (2003). Spatial organization of gene expression: the active chromatin hub. *Chromosome Res*. **11**, 447-459.

**Eskiw, C. H., Dellaire, G., Mymryk, J. S. and Bazett-Jones, D. P.** (2003). Size, position and dynamic behavior of PML nuclear bodies following cell stress as a paradigm for supramolecular trafficking and assembly. *J. Cell Sci.* **116**, 4455-4466.

**Eskiw, C. H., Dellaire, G. and Bazett-Jones, D. P.** (2004). Chromatin contributes to structural integrity of promyelocytic leukemia bodies through a SUMO-1-independent mechanism. *J. Biol. Chem*. **279**, 9577-9585.

**Fakan, S.** (2004). The functional architecture of the nucleus as analysed by ultrastructural cytochemistry. *Histochem. Cell Biol*. **122**, 83-93.

**Fakan, S., Puvion, E. and Spohr, G.** (1976). Localization and characterization of newly synthesized nuclear RNA in isolated rat hepatocytes. *Exp. Cell Res*. **99**, 155-164.

**Faro-Trindade, I. and Cook, P. R.** (2006a). A conserved organization of transcription during embryonic stem cell differentiation and in cells with high C value. *Mol. Biol. Cell* **17**, 2910-2920.

**Faro-Trindade, I. and Cook, P. R.** (2006b). Transcription factories: structures conserved during differentiation and evolution. *Biochem. Soc. Trans*. **34**, 1133-1137.

**Femino, A. M., Fay, F. S., Fogarty, K. and Singer, R. H.** (1998). Visualization of single RNA transcripts in situ. *Science* **280**, 585-590.

**Grande, M. A., van der Kraan, I., de Jong, L. and van Driel, R.** (1997). Nuclear distribution of transcription factors in relation to sites of transcription and RNA polymerase II. *J. Cell Sci.* **110**, 1781-1791.

**Hozák, P., Cook, P. R., Schöfer, C., Mosgöller, W. and Wachtler, F.** (1994). Site of transcription of ribosomal RNA and intra-nucleolar structure in HeLa cells. *J. Cell Sci*. **107**, 639-648.

**Iborra, F. J. and Cook, P. R.** (1998). The size of sites containing SR proteins in human nuclei: problems associated with characterizing small structures by immunogold labelling. *J. Histochem. Cytochem.* **46**, 985-992.

**Iborra, F. J., Pombo, A., Jackson, D. A. and Cook, P. R.** (1996). Active RNA polymerases are localized within discrete transcription 'factories' in human nuclei. *J. Cell Sci.* **109**, 1427-1436.

**Iborra, F. J., Jackson, D. A. and Cook, P. R.** (2000). Transport of mRNA through nuclear pores: apparent entry from the sides into dedicated pores. *J. Cell Sci*. **113**, 291-302.

**Jackson, D. A., Yuan, J. and Cook, P. R.** (1988). A gentle method for preparing cyto- and nucleo-skeletons and associated chromatin. *J. Cell Sci.* **90**, 365-378.

**Jackson, D. A., Hassan, A. B., Errington, R. J. and Cook, P. R.** (1993). Visualization of focal sites of transcription within human nuclei. *EMBO J.* **12**, 1059-1065.

**Jackson, D. A., Iborra, F. J., Manders, E. M. M. and Cook, P. R.** (1998). Numbers and organization of RNA polymerases, nascent transcripts and transcription units in HeLa nuclei. *Mol. Biol. Cell* **9**, 1523-1536.

**Kettenberger, H. and Cramer, P.** (2006). Fluorescence detection of nucleic acids and proteins in multi-component crystals. *Acta Crystallogr. D Biol. Crystallogr.* **62**, 146-150.

**Kornberg, R. D.** (2007). The molecular basis of eukaryotic transcription. *Proc. Natl. Acad. Sci. USA* **104**, 12955-12961.

**Kruhlak, M. J., Celeste, A., Dellaire, G., Fernandez-Capetillo, O., Muller, W. G., McNally, J. G., Bazett-Jones, D. P. and Nussenzweig, A.** (2006). Changes in chromatin structure and mobility in living cells at sites of DNA double-strand breaks. *J. Cell Biol*. **172**, 823-834.

**Luger, K., Mäder, A. W., Richmond, R. K., Sargent, D. F. and Richmond, T. J.** (1997). Crystal structure of the nucleosome core particle at 2.8 Å resolution. *Nature* **389**, 251-260.

**Marenduzzo, D., Faro-Trindade, I. and Cook, P. R.** (2007). What are the molecular ties that maintain genomic loops? *Trends Genet*. **23**, 126-133.

**Martin, S., Failla, A. V., Spori, U., Cremer, C. and Pombo, A.** (2004). Measuring the size of biological nanostructures with spatially modulated illumination microscopy. *Mol. Biol. Cell* **15**, 2449-2455.

**Misteli, T.** (2007). Beyond the sequence: cellular organization of genome function. *Cell* **128**, 787-800.

**Muller, W. G., Rieder, D., Karpova, T. S., John, S., Trajanoski, Z. and McNally, J. G.** (2007). Organization of chromatin and histone modifications at a transcription site. *J. Cell Biol*. **177**, 957-967.

**Olins, A. L., Olins, D. E. and Bazett-Jones, D. P.** (1992). Balbiani ring hnRNP substructure visualized by selective staining and electron spectroscopic imaging. *J. Cell Biol*. **117**, 483-491.

**Osborne, C. S., Chakalova, C., Brown, K. E., Carter, D., Horton, A., Debrand, E., Goyenechea, B., Mitchell, J. A., Lopes, S., Reik, W. et al.** (2004). Active genes dynamically co-localize to shared sites of ongoing transcription. *Nat. Genet*. **36**, 1065-1071.

**Politz, J. C., Polena, I., Trask, I., Bazett-Jones, D. P. and Pederson, T.** (2005). A nonribosomal landscape in the nucleolus revealed by the stem cell protein nucleostemin. *Mol. Biol. Cell* **16**, 3401-3410.

**Pombo, A., Hollinshead, M. and Cook, P. R.** (1999a). Bridging the resolution gap: imaging the same transcription factories in cryosections by light and electron microscopy. *J. Histochem. Cytochem*. **47**, 471-480.

**Pombo, A., Jackson, D. A., Hollinshead, M., Wang, Z., Roeder, R. G. and Cook, P. R.** (1999b). Regional specialization in human nuclei: visualization of discrete sites of transcription by RNA polymerase III. *EMBO J*. **18**, 2241-2253.

**Rasband, W. S.** (1997-2007). ImageJ, http://rsb.info.nih.gov/ij/. Bethesda, MD: US National Institutes of Health.

**Ren, Y., Kruhlak, M. J. and Bazett-Jones, D. P.** (2003). Same serial section correlative light and energy-filtered transmission electron microscopy. *J. Histochem. Cytochem*. **51**, 605-612.

**Sadoni, N. and Zink, D.** (2004). Nascent RNA synthesis in the context of chromatin architecture. *Chromosome Res.* **12**, 439-451.

**Simonis, M., Klous, P., Splinter, E., Moshkin, Y., Willemsen, R., de Wit, E., van Steensel, B. and de Laat, W.** (2006). Nuclear organization of active and inactive chromatin domains uncovered by chromosome conformation capture-on-chip (4C). *Nat. Genet*. **38**, 1348-1354.

**Wansink, D. G., Schul, W., van der Kraan, I., van Steensel, B., van Driel, R. and de Jong, L.** (1993). Fluorescent labelling of nascent RNA reveals transcription by RNA polymerase II in domains scattered throughout the nucleus. *J. Cell Biol*. **122**, 283-293.

**Weibel, E. R.** (1979). *Stereological Methods: Practical Methods for Biological Morphometry*. London: Academic Press.

**Wetterberg, I., Zhao, J., Masich, S., Wieslander, L. and Skoglund, U.** (2001). *In situ* transcription and splicing in the Balbiani ring 3 gene. *EMBO J.* **20**, 2564-2574.

**Williams, M. A.** (1977). Quantitative methods in biology. In *Practical Methods in Electron Microscopy* (ed. A. M. Glauert), pp. 5-84. Amsterdam: North-Holland.

Journal of Cell Science